

**OMAE2011-50171**

**CORROSION-FATIGUE PERFORMANCE OF HIGH-STRENGTH RISER STEELS  
IN SEAWATER AND SOUR BRINE ENVIRONMENTS**

**Stephen J. Hudak, Jr.<sup>1</sup>, Guadalupe B. Robledo<sup>1</sup>, and Jeffrey Hawk<sup>2</sup>**

<sup>1</sup>Southwest Research Institute® (SwRI), San Antonio, Texas, USA

<sup>2</sup>National Energy Technology Lab (NETL), Albany, Oregon, USA

**ABSTRACT**

Although new high-strength steels have recently been developed to meet the demands of increased reservoir pressures, and sour production fluids, the corrosion-fatigue performance of these new higher-strength materials is largely unknown. The goal of this study was to fill this knowledge gap by generating corrosion-fatigue data in two aggressive environments: 1) a sour production brine, and 2) seawater with cathodic protection. The focus of the current paper is on stress-life (S-N) corrosion-fatigue results in these environments, as well as a baseline air environment. Experiments were performed on five different steels with yield strengths ranging from 848 MPa to 1080 MPa. Prior frequency-scan results based on corrosion-fatigue crack growth rate data demonstrated that not all of these material-environment combinations exhibit a saturation frequency where the detrimental environmental effect approached a constant value as the cyclic loading frequency is decreased. Consequently, S-N tests were performed at different frequencies (0.01 Hz, 0.17 Hz, and 1 Hz), depending on the fatigue life regime, in attempting to match the loading frequencies experienced in service. Corrosion-fatigue occurred at stresses well below the fatigue endurance limit in laboratory air, and cyclic lives in the seawater with cathodic protection environment were found to be 2X to 10X less than those in the baseline air environment, while cyclic lives in the sour brine environment were found to be 30X to 100X less than those in the baseline air environment. In both environments, degradation was greatest at lower stresses in the high cycle fatigue regime. The effect of material strength level had little or no measurable effect on the S-N corrosion-fatigue performance, and the effect of cyclic frequency on the corrosion-fatigue performance was mixed. The S-N response to these two variables differed significantly from recently measured fatigue crack growth kinetics in these same materials that were performed in a companion study. Possible reasons for these differences are discussed.

**INTRODUCTION**

Corrosion-fatigue is a significant design consideration in deepwater floating production systems. In these structures, fatigue loading is accentuated due the compliant nature of the structures; moreover, sour-service conditions can also be experienced either due to the nature of the original production fluid, or due to seawater flooding of the reservoir to enhance production yield. When currently used riser materials (X65 and X70 steels) are exposed to sour brine environments, they can exhibit reductions in the fatigue life by factors of 10X to 100X compared to the fatigue life in laboratory air [1-7]. Moreover, the extent of degradation is dependent on the cyclic loading frequency and typically increases with decreasing cyclic frequency due to the time-dependent nature of the material-environment interaction. Thus, ideally tests need to be conducted at or near the cyclic loading frequency experienced in the structure – typically 0.01 to 0.33 Hz.

Higher-strength steel risers have been developed recently to meet the requirements of deep water and hostile environments. However, information is lacking on corrosion-fatigue performance of these new materials in representative service environments. The research summarized in this paper represents a portion of the work sponsored by the U.S. Dept. of Energy through the National Energy Technology Laboratory (NETL) under the RPSEA Program. The goal of this program is to generate corrosion-fatigue data to fill this information gap on these new materials.

**OBJECTIVE AND APPROACH**

The specific objective of this study was to quantify the affect of applied stress, environment, and material strength level on corrosion-fatigue life. Limited data were also obtained on the effect of cyclic loading frequency on S-N corrosion-fatigue life.

The experimental approach was to first identify the frequency response of the various material-environment

combinations using frequency-scan experiments conducted over a range of frequencies and a fixed crack-tip “driving force” employing a technique that has previously been described in Refs. [8-10]. These experiments were performed in a companion study on the same five steels and environments as those of the current study, and have been previously reported in Ref. [11]. In these previous frequency scan experiments, crack-driving force was characterized in terms of the range of crack-tip stress intensity factor ( $\Delta K$ ) defined by linear elasticity. The objective of these tests was to define an optimum test frequency in order to ensure that laboratory-generated data would be representative of service-loading conditions, while at the same time do not result in impractical test durations. These results were then used to formulate a testing strategy for generating corrosion-fatigue crack growth rates over a wide range of applied stress range and corrosion-fatigue life.

However, as shown in Figures 1 and 2 from a companion study [11], not all material-environment combinations of interest here exhibited a saturation frequency, thus an optimum frequency could not be defined and used for all materials and environments in the current S-N testing.

Consequently, a variable-frequency testing strategy was employed in the current study that attempted to match the loading frequency experienced by structures in service for various fatigue life regimes. The lowest frequency (0.01 Hz) was applied at high stresses in the low-cycle fatigue regime in attempting to simulate loading such as thermal fatigue associated with stop-start cycles, while a higher frequency (0.17 Hz) was applied at intermediate stresses in the intermediate-cycle fatigue regime to simulate stresses generated by wave-induced vessel motions and vortex-induced vibrations, and a higher frequency (1 Hz) was applied in the low stress, high-cycle fatigue regime. The latter frequency was a practical expedient; otherwise, corrosion-fatigue data could not have been obtained in this life regime in a reasonable time. Limited overlapping data (i.e., data at the same stress and two different frequencies) were obtained at the boundaries of these regimes in order to better understand the effect of frequency on S-N corrosion-fatigue performance.

### MATERIALS, SPECIMENS AND ENVIRONMENTS

The test materials were carbon-manganese steels and were supplied by various pipe manufacturers in the form of seamless pipe in various diameters and thicknesses, as shown in Figure 3. These high-strength pipes did not contain welds since welding procedures are not available for steels at these high-strength levels. Consequently, their application as risers will likely involve joining using threaded connections.

The tensile properties of the five steels are summarized in Table 1. As can be seen, the yield strengths varied by about 27%, ranging from 848 MPa to 1080 MPa. Although the tensile ductilities, as measured by percent elongation and

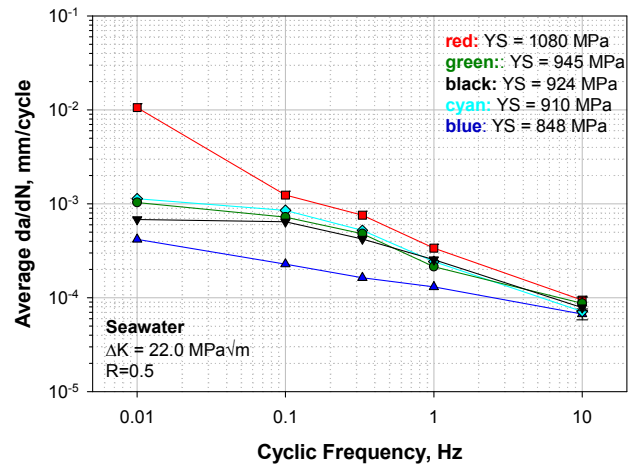


**FIGURE 1: FREQUENCY SCAN RESULTS IN SEAWATER WITH CATHODIC PROTECTION SHOWING LACK OF A SATURATION FREQUENCY AT LOW FREQUENCY FOR CERTAIN YIELD STRENGTH (YS) STEELS (from Ref. 11).**

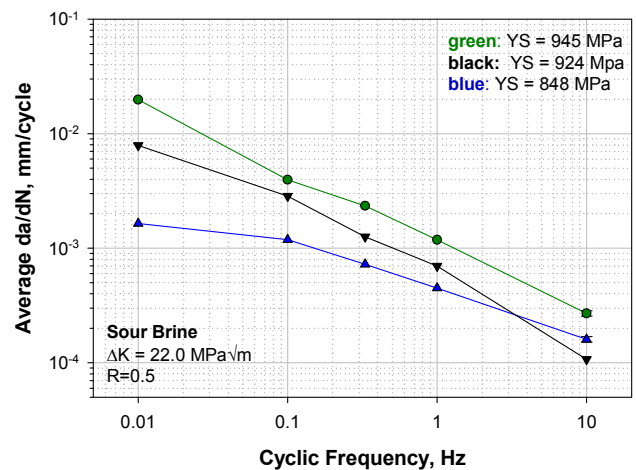


**FIGURE 2: FREQUENCY SCAN RESULTS IN SOUR BRINE SHOWING LACK OF A SATURATION FREQUENCY AT LOW FREQUENCY FOR CERTAIN YIELD STRENGTH (YS) STEELS (from Ref. 11).**

percent reduction in area, tended to decrease with increasing strength level, all of the steels exhibited good ductility.

Full-thickness strip fatigue specimens were extracted from the pipes as illustrated in Figure 4. The number of specimens that could be excised from a given pipe segment varied between three-to-five, depending on the pipe diameter. In the gage section of the specimens, the specimen width was equal to the thickness, which ranged from 14 mm to 33 mm. This was done to limit the load capacity required for fatigue testing in these high-strength steels – particularly for the baseline testing in air where the fatigue endurance limit is typically proportional to the ultimate strength of the



**FIGURE 3: TEST PIPES WITH OUTER DIAMETERS RANGING FROM 284 mm TO 406 mm AND WALL THICKNESS FROM 14 mm TO 34 mm.**

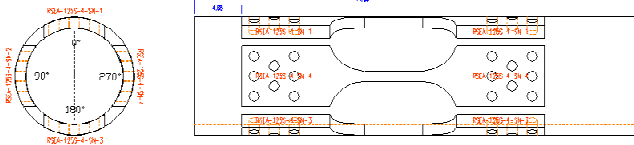


**FIGURE 4: S-N FATIGUE STRIP SPECIMEN AND EXAMPLE PLAN FOR THEIR REMOVAL FROM PIPE. DEPENDING ON PIPE DIAMETER, THREE-TO-FIVE SPECIMENS WERE REMOVED FROM EACH PIPE SEGMENT.**

steel. The use of a specimen of width equal to the pipe thickness is not advisable when fatigue testing welded pipe material where it is important to sample an adequate length of weld in order to generate representative fatigue properties.

However, in the present test this was not an important consideration since all tests were on base material – that is, without welds. As discussed later, the fatigue results support the validity of this approach.

S-N fatigue data were generated in three environments: 1) a laboratory air environment to provide a baseline for comparison of the effects of the more aggressive environments; 2) a simulated seawater (SW) environment, which was prepared per ASTM D1141 and open to the air, and included cathodic protection of -1050 mv versus the Standard Calomel Electrode, to represent the external environment of the riser typical of near-surface or splash zone; and 3) a sour brine (SB) environment, which was prepared with a production brine with 35% H<sub>2</sub>S and 65% CO<sub>2</sub> and oxygen below 10 ppb to represent the internal environment of the riser with very low oxygen typical of the production fluid. However, as indicated in Table 1, only two of the five steels were tested in the SB environment since not all steels were intended for use in sour service.

### EXPERIMENTAL PROCEDURE

The S-N fatigue data were generated using constant-amplitude applied stress ranges from 900 MPa to about 75 MPa. All tests were performed at a stress ratio (R = minimum stress/maximum stress) of 0.1. These stresses resulted in fatigue lives from 5,000 cycles to 10 million cycles.

Tests conducted in the air environment used relatively high cyclic loading frequencies (2-3 Hz) to expedite the data generation since steels tested in air are relatively insensitive to cyclic loading frequency; thus, it was not necessary to test at lower frequencies. As previously discussed, tests conducted in the seawater plus cathodic protection and in the sour brine environments used frequencies of 0.01 Hz, 0.17 Hz, or 1 Hz, depending on the applied stress and life regime. Specifically, the life regimes for the different frequencies were 0.01 Hz: 5,000-60,000 cycles; 0.17 Hz: 26,000-1,600,000 cycles, and 1 Hz: 165,000-10,000,000 cycles.

**TABLE 1: AVERAGE TENSILE PROPERTIES OF THE FIVE HIGH-STRENGTH STEELS TESTED IN THE CURRENT PROGRAM AND CORRESPONDING TEST ENVIRONMENTS.**

Yield Strength (YS) MPa	Ultimate Strength (UTS) MPa	Percent Elongation	Percent Reduction in Area	Test Environments	
				SW	SB
848	862	23.7	71.1	X	X
910	993	19.2	65.8	X	
924	1000	22.1	62.7	X	
945	1000	20.5	66.8	X	X
1080	1160	18.5	65.4	X	

The United States Government retains, and by accepting the article for publication, the publisher acknowledges that the U.S. Government retains, a non-exclusive, paid-up, irrevocable, worldwide license to publish or reproduce the published form of this work, or allow others to do so, for U.S. Government purposes.

A “runout” test was defined as a test that survived 10,000,000 cycles. These frequencies and fatigue lives resulted in individual test durations from one week to nearly six months.

Corrosion-fatigue testing in the seawater environment was conducted in a polymeric chamber that was open to the laboratory air since it was designed to simulate seawater near the surface and in the splash zone where high fatigue bending stresses are typically experienced in risers during service.

Corrosion-fatigue testing in the sour brine environment was conducted in a specially-designed facility consisting of environmental chambers, gas delivery systems, and safety systems. The safety system contained sensors and alarms to provide automatic shutdown of the gas supply system in the event of a test gas leak. For both safety, as well as to maintain low oxygen levels (less than 10 ppb), the sour brine environment enclosure consists of a triple containment system, which was comprised of a primary chamber, a shroud, and an exhaust enclosure, as shown in Figure 5.

The innermost primary chamber contained the specimen and the sour brine test solution, and was constructed of a nickel-based alloy for corrosion resistance. This chamber was electrically isolated from the specimen to prevent galvanic corrosion of the specimen. The shroud provided secondary containment and was constructed of a 10-mil thick transparent, flexible polymeric tube connected to two aluminum flanges attached to the upper and lower specimen grips. The shroud was filled with flowing  $N_2$  gas to provide a further barrier to diffusion of  $O_2$  into the primary chamber during testing. The shroud also served as a barrier to contain any sour gas that might escape from the primary chamber, should the primary chamber seal system fail during testing. For this reason, the shroud also housed an  $H_2S$  detector, which was connected to an alarm/shutdown panel that was used to stop the flow of the test gas into the primary chamber in the event of a primary chamber leak.

The third barrier consisted of an acrylic and aluminum exhaust enclosure that surrounded the central portion of the test frame. This enclosure was connected to a roof-mounted duct system that provided continuous evacuation of the enclosure during sour gas testing. The enclosure also served as a platform to mount hardware associated with the test gas and test solution delivery lines (tubing), flow meters and valves. The flow rate of each gas stream within the test chamber was controlled by means of rotameters, with the maximum flow through each of approximately 125 ml/min at a supply pressure of 15 psi. The gas leaving the test chamber passed through  $\frac{3}{4}$ -inch PVC tubing in the hydraulic system trenching to a gas scrubber outside the lab, which contained an aqueous caustic solution (NaOH) to reduce the  $H_2S$  gas to a non-toxic sulfide compound.

The gas exiting the scrubber passed through a bed of activated charcoal to remove trace amounts of  $H_2S$ , and was then evacuated through a roof-mounted ventilation system

and stack. Solenoid valves are located within each test frame enclosure and on the gas delivery manifold outside of the test laboratory. The monitor/alarm panel automatically controls the operation of each flow shutoff valve. Additionally, the system is designed to be failsafe in the event of loss of air supply or control panel power to the Uninterruptable Power Supply (UPS).

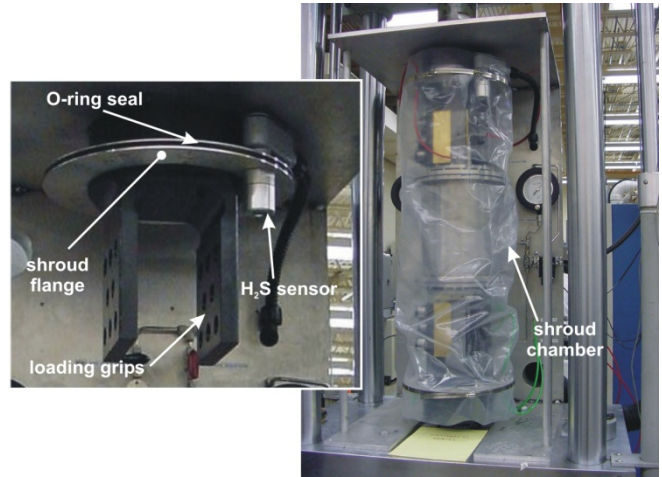


**FIGURE 5: CORROSION-FATIGUE TEST SET-UP SHOWING PRIMARY CHAMBER, SHROUD AND EXTERNAL ALUMINUM FRAME OF EXHAUST ENCLOSURE (ACRYLIC WALLS NOT SHOWN); ALSO SHOWN ARE LOADING GRIP, SHROUD SEAL, AND  $H_2S$  SENSOR.**

## RESULTS AND DISCUSSION

This section first presents the S-N fatigue data in the baseline laboratory-air environment, followed by the results in seawater with cathodic protection (SW) and in sour brine (SB) environments.

### S-N Fatigue in Lab Air

Most of the baseline air data were generated at the DOE’s National Energy Technology Laboratory (NETL). Selected air data were also generated at Southwest Research Institute on the 848 MPa YS steel in order to compare with the NETL-generated data on the same steel, and thereby assess the inter-laboratory reproducibility of results. These results are shown in Figure 6 and can be seen to exhibit good agreement between the two laboratories, particularly considering the typical scatter in S-N fatigue data.

Figure 7 compares all available air S-N fatigue data for the steels of different strength levels. As indicated by the data, there was no measurable difference among the S-N fatigue lives for the steels with yield strengths ranging from 848 MPa to 945 MPa YS; however the 1080 MPa YS data exhibited noticeably longer fatigue lives. Moreover, close examination of the data beyond 1 million cycles indicated about a 30% higher fatigue endurance limit at 10 million

cycles for both the 945 MPa and 1080 MPa YS steels compared to the lower strength steels. This trend of increasing fatigue endurance limit with increasing strength is well known for materials tested in benign environments, which is largely the case for steels tested in laboratory air. This increase in fatigue endurance limit may also be due to differences in steel microstructure; although this assessment remains to be done. The fact that the current results on the three lowest strength steels (848 MPa to 924 MPa) do not exhibit different fatigue endurance limits is likely due to their small difference (9%) in nominal strength level.

Figure 7 also shows the trend line for the air data obtained by linear regression analysis using the applied stress as the independent variable and the fatigue life as the dependent variable. This analysis was limited to data with fatigue lives less than one million cycles where the S-N results are linear in log-log space and thus can be properly represented by a power law. The regression parameters for this power law fit are as follows:

$$N_f = 2 \times 10^{17} (\Delta\sigma)^{-4.486} \quad [1]$$

Equation 1 will be used as the basis for comparing the relative extent of environmental degradation due to both the seawater and sour brine environments.

### S-N Fatigue in Seawater

A summary of the S-N fatigue data in air versus seawater with cathodic protection is provided in Figure 8. Note the difference in slopes of the results in the two different environments, which results in the seawater with cathodic protection data converging with the air data at high stress and low fatigue lives. This slope difference is a manifestation of the fact that the degradation in fatigue life due to the interaction of the material and seawater environment varies with applied stress range – specifically, from less than a factor of two at high stress ranges to about a factor of ten at lower stress ranges and longer lives.

### S-N Fatigue in Sour Brine Environment

A summary of the S-N fatigue data in air versus sour brine environments is provided in Figure 9. The slope of the sour brine curve differs from that of the air curve but the slope difference is much less pronounced than that exhibited by the seawater versus air data shown in Figure 8. Consequently, the sour brine and air curves do not converge even if the curves are extrapolated back to very small fatigue lives (e.g., 100 cycles). At applied stress ranges of 500 MPa, 400 MPa, and 200 MPa, the corrosion-fatigue lives in sour brine are respectively 30X, 50X, and 100X less than those in laboratory air (given by Equation 1).

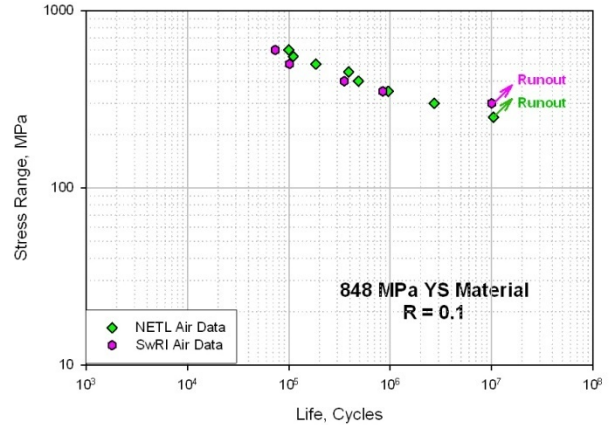


FIGURE 6: COMPARISON OF AIR-BASELINE S-N FATIGUE DATA GENERATED AT SwRI AND AT NETL.

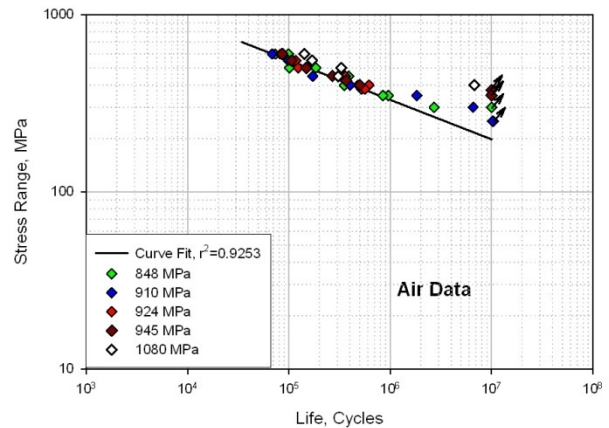


FIGURE 7: COMPARISON OF AIR BASELINE S-N FATIGUE DATA FOR FIVE STEELS AT VARIOUS STRENGTH LEVELS. [Reviewers' Note: Data for 1080 MPa steel to be added when available.]

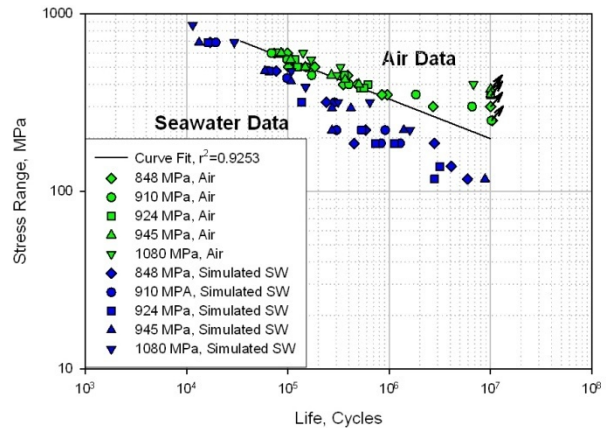
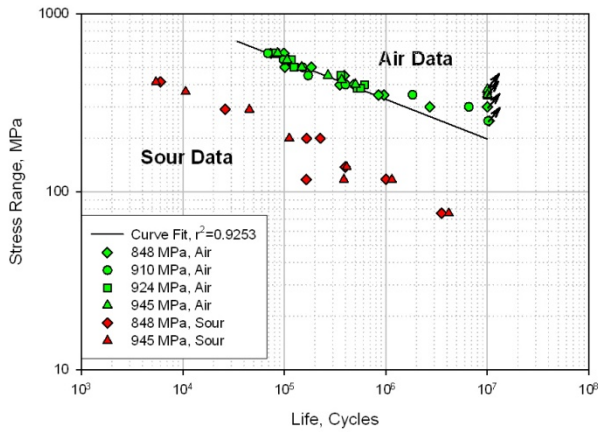
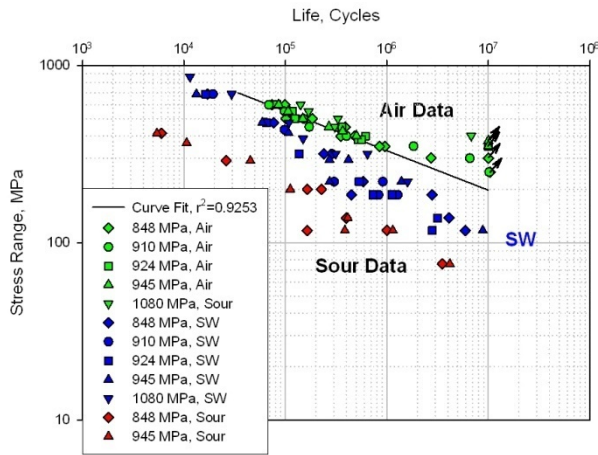


FIGURE 8: COMPARISON OF S-N FATIGUE DATA IN BASELINE AIR AND SEAWATER WITH CATHODIC PROTECTION ENVIRONMENTS.

Figure 10 provides a summary of the S-N fatigue data in sour brine, seawater with cathodic protection, and laboratory air environments. The difference in slopes between the sour brine and seawater with cathodic protection data causes more significant differences between these two curves at higher stress ranges in the low-cycle-fatigue-regime than at lower stress ranges in the high-cycle-fatigue regime. Also, there are little or no discernable differences in the corrosion-fatigue lives in any of the environments as a function of material strength level. This trend differs with that observed in corrosion-fatigue crack growth kinetics [11].



**FIGURE 9: COMPARISON OF S-N FATIGUE DATA IN BASELINE AIR AND SOUR BRINE ENVIRONMENTS.**



**FIGURE 10: COMPARISON OF S-N FATIGUE DATA IN AIR, SEAWATER WITH CATHODIC PROTECTION, AND IN SOUR BRINE ENVIRONMENTS.**

**Effect of Frequency on Corrosion-Fatigue Life**

The possible effect of cyclic loading frequency on the S-N fatigue response in sour brine and in seawater with cathodic protection was also examined.

In Figure 10, for stress ranges between 186 MPa and 317 MPa, there are seven cases where more than one life

occurs at a given stress range and for a given steel exposed to the seawater with cathodic protection environment – this is due to the fact that two different loading frequencies were used at the same stress level. Similarly, for stresses between 117 MPa and 200 MPa there are three cases where more than one life occurs at a given stress range for a given steel exposed to the sour brine environment. Using these data, the effect of frequency on corrosion-fatigue life can be more clearly seen in the summary graphs of Figures 11 and 12, where results are presented in terms of a fatigue life ratio (FLR), which is defined here as the fatigue life at 0.01 Hz divided by that at 1 Hz, for a given material, environment, and applied stress range. Thus,  $FLR < 1$  indicates that the fatigue life decreases with decreasing frequency (the so-called classical frequency effect), and  $FLR > 1$  indicates that the fatigue life increases with decreasing frequency (the so-called inverse frequency effect [11]). For  $FLR = 1$ , the fatigue lives would be independent of cyclic frequency.

Based on data obtained in the seawater with cathodic protection environment in Figure 11, five of the seven cases indicate a classical frequency effect, while two of the seven cases indicate an inverse frequency effect. In addition, the classical frequency effect is favored at low stress ranges (186 MPa to 221 MPa) while the inverse frequency effect is favored at high stress ranges (294 MPa and 317 MPa). Interestingly, this trend is opposite to that which was recently reported for corrosion-fatigue crack growth kinetics in the same steels and environments [11].

Based on data obtained in the sour brine environment in Figure 12, the three cases are evenly split with one indicating a classical frequency effect ( $FLR = 0.28$ ), one an inverse frequency effect ( $FLR = 6.1$ ), and one indicating little or no influence of frequency ( $FLR = 1.36$ ).

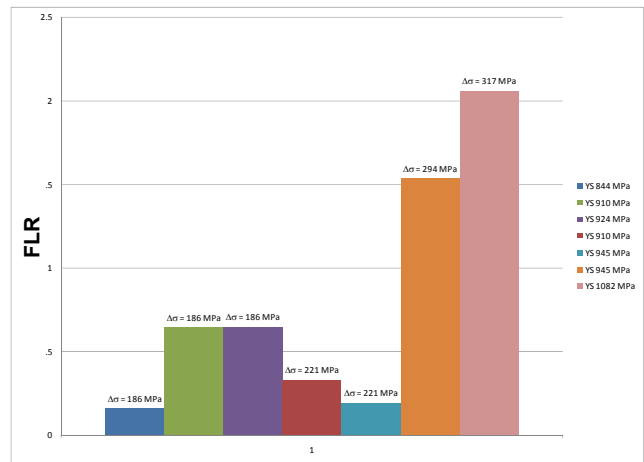


**FIGURE 11: CORROSION-FATIGUE LIFE RATIOS (FLRs) FOR 0.17-Hz/1-Hz DATA IN THE SEAWATER WITH CATHODIC PROTECTION ENVIRONMENT AT VARIOUS APPLIED STRESS RANGES FOR DIFFERENT STEEL STRENGTH LEVELS.**

The United States Government retains, and by accepting the article for publication, the publisher acknowledges that the U.S. Government retains, a non-exclusive, paid-up, irrevocable, worldwide license to publish or reproduce the published form of this work, or allow others to do so, for U.S. Government purposes.

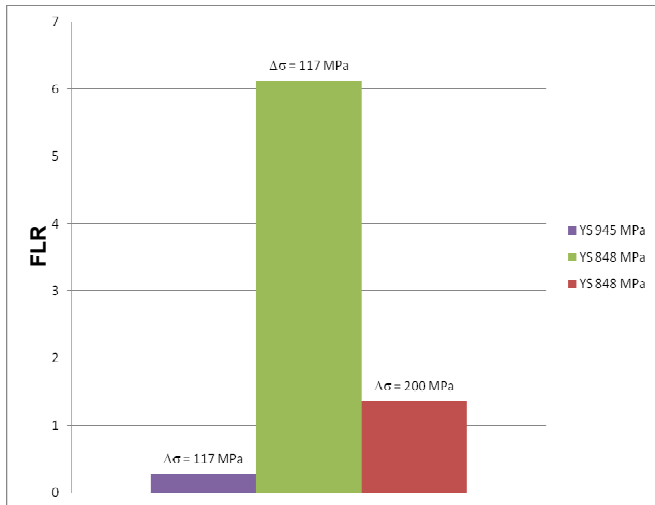


**FIGURE 12: CORROSION-FATIGUE LIFE RATIOS (FLRs) FOR 0.17 Hz/1 Hz DATA IN THE SOUR BRINE ENVIRONMENT AT VARIOUS APPLIED STRESS RANGES FOR DIFFERENT STEEL STRENGTH LEVELS.**

## DISCUSSION

It is of interest to note that the trends exhibited in the current S-N corrosion-fatigue results with respect to both strength level and cyclic loading frequency differ from those exhibited by fatigue crack growth rates in these same steels. We can offer two hypotheses to explain these apparent differences between S-N corrosion-fatigue and corrosion-fatigue crack growth kinetics.

The first hypothesis is that in the current case the S-N corrosion-fatigue life, which in general consists of both a fatigue crack initiation component and a fatigue crack growth component, is in fact controlled by the initiation component. And in addition, the material-environment interaction during the corrosion-fatigue initiation component is fundamentally different than that which occurs during the corrosion-fatigue crack growth component. This hypothesis would be favored by the fact that the current results were obtained on base materials, as compared to weldments. Under these conditions, the fatigue initiation life of S-N specimens would be expected to play a more dominant role in controlling the overall fatigue life since the fatigue specimen would not have contained significant initial defects that would preclude a significant crack initiation phase – for example, as typically occurs in welded specimens. Instead, the predominant fatigue crack initiation location in these base-metal, S-N specimens was observed to occur at the edge of the specimen. Crack initiation was observed to occur preferentially at this location even though the originally sharp edge resulting from initial machining was ground and polished by hand in attempting to remove possible machining defects, although the effectiveness of this specimen preparation procedure cannot guarantee the

removal of all small machining defects. Nevertheless, crack initiation at the specimen edge is also likely to have been promoted due to the lack of constraint at the intersection of the two surfaces, which would give rise to slightly higher strains compared to the nominal strain that existed in the remainder of the specimen.

An alternative hypothesis is that the corrosion-fatigue life in the S-N strip specimens were in fact dominated by fatigue crack growth; however, the noted difference in sensitivity to strength level and cyclic loading frequency between the S-N specimens and the crack growth specimens was due to a crack size/geometry effect – specifically, the difference between small edge, or surface, cracks in the S-N specimen versus the long, through-thickness cracks in fatigue crack growth rate specimens. Such crack size/geometry effects have previously been reported to cause differences in corrosion-fatigue crack growth kinetics ( $da/dN$  vs.  $\Delta K$ ). Specifically, small surface cracks (0.1 - 1 mm) in high-strength, low-alloy steels exposed to 3.5% sodium chloride environments have been shown to grow at significantly faster rates compared to long, through-thickness cracks (25 - 40 mm) in conventional fracture mechanics specimens [12-13]. It has been proposed that this difference in growth rates is due to the effect of the crack size/geometry differences on mass transport within the crack, which causes changes in the occluded environment at the crack tip [13-14]. However, this environmental small crack effect has not, to our knowledge, been systematically examined as a function of material strength level or cyclic loading frequency. Thus, further research is needed to elucidate the causes of these differences between S-N corrosion-fatigue lives and corrosion-fatigue crack growth kinetics.

On a more pragmatic level, it is of interest to compare the current S-N fatigue results on high-strength riser steels with available results on X65/X70 steels tested in both air and sour brine environments [7, 10, and 15]. This comparison for results tested in lab air is shown in Figure 13. In interpreting these results it is important to recognize that the current high-strength steels results are in the un-welded condition, while the low-strength X65/X70 steels are all in the welded condition. There are no results on welded high-strength steels since a viable weld procedure has not yet been developed for these high-strength steels, thus initial applications of these materials will employ threaded connections.

As can be seen in Figure 13, the low-strength steel results vary significantly, and this is primarily due to variations in the welding process employed. The most dramatic effect can be seen in the results labeled SwRI-Tenaris for which the weld root and cap were removed using a flapping process [15], which resulted in a fatigue endurance limit at 10 million cycles comparable to the current un-welded results on high-strength steels. These results suggest that much of the detrimental results of welds

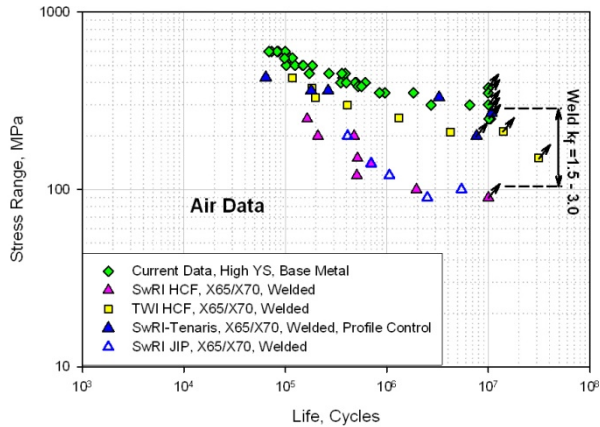


**FIGURE 13: COMPARISON OF CURRENT HIGH-STRENGTH STEEL DATA WITH AVAILABLE X65/X70 DATA IN LAB AIR**

are due to the geometrical stress concentration of the weld root and cap. The flapping process is also believed to impart a near-surface residual compressive stress in the material, and this may also explain why the endurance limits for these low-strength (448-483 MPa YS) and high-strength (848-924 MPa YS) steels are similar – that is, they do not follow the strength level dependence of the fatigue endurance limit exhibited by the current results shown in Figure 7.

Based on the above discussion, if we now assume that the flapping process restores the welded fatigue properties to those of the un-welded condition, we can compute effective fatigue notch reduction factors,  $k_f$ , at 10 million cycles for the various welded S-N curves. As indicated in Figure 13, this gives  $k_f$  values ranging from 1.5 to 3.0.

Figure 14 compares the current S-N corrosion fatigue data in sour brine with available sour brine data on welded X65/X70 data. As can be seen, the unadjusted comparison shows that the current high-strength data have longer corrosion fatigue lives than those of the welded X65/X70 corrosion fatigue lives. However, since the later results include the influence of welds, as well as the sour brine environment, a more fair comparison would need to adjust the high-strength data for the threaded connection method that will be employed to join these pipes in service. A first order estimate of this effect on the high-strength steels fatigue lives can be made by assuming an appropriate  $k_f$  value for the threaded connections will be in the range of those determined above for the welded connection ( $k_f = 1.5$  to 3.0 in Figure 13). Applying this range of knock-down factors on stress gives the solid lines shown in Figure 14, which can be considered to be a first order estimate of the combined effect of the sour brine environment and threaded connections in high-strength steels. This estimate provides an initial comparison of current riser technology (i.e. welded connections in low-strength steels) versus future riser

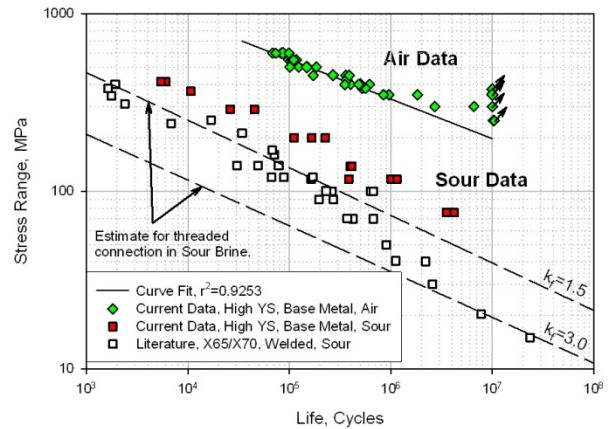


**FIGURE 14: COMPARISON OF ESTIMATED SOUR BRINE FATIGUE PERFORMANCE OF HIGH-STRENGTH STEEL WITH THREADED CONNECTIONS VERSUS SOUR BRINE FATIGUE PERFORMANCE OF WELDED X65/X70 STEEL.**

technology (i.e. threaded connections in high-strength steels) for deepwater application. While it is understood that these threaded connections would likely contain seals to prevent ingress of the sour brine environment, the above estimated fatigue performance would nevertheless be useful for initial assessment of remaining fatigue life when considering the possibility that the seal is compromised, thereby exposing the threaded connection to the sour brine environment. Of course, this estimate should be verified by performing full-scale fatigue testing on high-strength threaded connections in sour brine environment. However, a number of technical challenges that would need to be overcome before such data could be obtained.

## SUMMARY AND CONCLUSIONS

1. Fatigue lives in air were observed to be independent of material strength level over the range of yield strengths from 848 MPa to 945 MPa, although fatigue lives were measurably longer for the highest yield strength material at 1080 MPa.
2. The fatigue endurance limit at  $10^7$  cycles in air was about 300 MPa and independent of strength level for yield strengths ranging from 848 MPa to 924 MPa, while it was above 400 MPa for yield strengths of 945 MPa and 1080 MPa.
3. Corrosion-fatigue lives in the seawater with cathodic protection were 2X to 10X less than those measured in air, and this difference increased with decreased applied stress range.
4. Corrosion-fatigue lives in the sour brine environment were 30X to 100X less than those measured in air, and this difference increased with decreasing applied stress range, as in the seawater environment.
5. Corrosion-fatigue occurred in seawater with cathodic protection and in sour brine at stresses significantly

below the fatigue endurance limit at 10 million cycles in air.

6. Corrosion-fatigue S-N behavior exhibited no measurable differences as a function of material strength level for yield strengths from 848 MPa to 1080 MPa in the seawater with cathodic protection environment and for yield strengths from 848 MPa to 945 MPa in the sour brine environment.
7. The effect of cyclic frequency on corrosion-fatigue behavior was mixed and exhibited both the classic frequency effect with lives decreasing with decreasing frequency, as well as the inverse frequency effect with lives decreasing with increasing frequency, although the effect of frequency was likely confounded by the inherent scatter in the S-N measurements.
8. Corrosion-fatigue lives in S-N tests were considerably less sensitive to steel strength level and cyclic loading frequency than were recently measured fatigue crack growth rate kinetics ( $da/dN$  vs.  $\Delta K$ ) in these same steels and environments [11].
9. Although several hypotheses were proposed to explain the above differences, the fundamental understanding and critical experimental results need to elucidate these differences are presently lacking.

#### ACKNOWLEDGEMENT

The support of the Research Partnership to Secure Energy for America (RPSEA) under prime contact with the U.S. Dept. of Energy (Contract DE-AC26-07NT42677), as well as co-funding from BP, is gratefully acknowledged. We are also grateful for the support and encouragement of James Pappas of RPSEA and Jim Chitwood of Chevron, who are respectively the current and past managers of the RPSEA Ultra-Deepwater Floating Facilities Project 1403. The contributions of Steven Shademan and Himanshu Gupta, both of BP, who co-chair the Project Working Committee, are also acknowledged.

#### REFERENCES

- [1] Buitrago, J. and Weir, M.S., 2002, "Experimental Fatigue Evaluation of Deepwater Risers in Mild Sour Environment," Deep Offshore Technology Conf., New Orleans, LA.
- [2] Baxter, D.P., Maddox, S.J., and Pargeter, R.J., 2007, "Corrosion Fatigue Behavior of Welded Risers and Pipelines," OMAE2007-29360, 26th Int'l. Conf. on Offshore Mechanics and Arctic Engineering, San Diego, CA.
- [3] McMaster, F., Thompson, H., Zhang, M., Walters, D., and Bowman, J., 2007, "Sour Service Corrosion Fatigue Testing of Flowline Welds," OMAE2007-29060, 26th Int'l. Conf. on Offshore Mechanics and Arctic Engineering, San Diego, CA.
- [4] Buitrago, J., Hudak, S.J. Jr., and Baxter, D., 2008, "High-Cycle and Low-Cycle Fatigue Resistance of Girth Welds in Sour Service," OMAE2008-57545, 27<sup>th</sup> Int'l. Conf. on Offshore Mechanics and Arctic Engineering, Estoril, Portugal.
- [5] McMaster, F., Bowman, J., Thompson, H., Zhang, M., and Kinyon, S., 2008, "Sour Service Corrosion Fatigue Testing of Flowline and Riser Welds," OMAE2008-57059, 27<sup>th</sup> Int'l. Conf. on Offshore Mechanics and Arctic Engineering, Estoril, Portugal.
- [6] Hudak, S.J. Jr. and McMaster, F., 2003, "Corrosion-Fatigue of Carbon Steel Weldments in Sour Environments," Final Report, SwRI Project No. 18.04860, Southwest Research Institute, San Antonio, TX.
- [7] Hudak, S.J. Jr., Chell, G., and Long, R., 2008, "Validation of a Methodology for Assessing Defect Tolerance of Welded Reeled Risers and Flowlines," Final Report – JIP on Reeling, SwRI Project No. 18.10265, Southwest Research Institute, San Antonio, TX.
- [8] Bartlett, M.L. and Hudak, S.J. Jr., 1990, "The Influence of Frequency-Dependent Crack Closure on Corrosion Fatigue Crack Growth," Fatigue '90, pp. 1783-1788.
- [9] Hudak, S.J. Jr., Birring, A.S., Bartlett, M.L., and Hanley, J.J., 1990, "Control of Corrosion-Fatigue in NGV Fuel Cylinders," SwRI Project No. 06-1566, GRI Contract No. 5086-252-1440, GRI-89/0239, Southwest Research Institute, San Antonio, Texas.
- [10] Buitrago, J., Weir, M.S., Kan, W.C., Hudak, S.J. Jr., and McMaster, F., 2004, "Effect of Loading Frequency on Fatigue Performance of Risers in Sour Environment," Offshore Mechanics and Arctic Engineering Conf., OMAE 2004-51641, Vancouver.
- [11] Hudak, S.J. Jr., Feiger, J.H., Patton, J.A., 2010, "The Effect of Cyclic Loading Frequency on Corrosion-Fatigue Crack Growth in High-Strength Riser Materials, 29<sup>th</sup> Int'l. Conf. on Offshore Mechanics and Arctic Engineering, OMAE2010-20705, Shanghai.
- [12] Gangloff, R.P., 1981, "The Criticality of Crack Size in Aqueous Corrosion Fatigue," *Research Mechanical Letters*, Vol. 1, pp. 299-306.
- [13] Gangloff, R.P., 1985, "Effect of Crack Size on the Chemical Driving Force for Corrosion Fatigue," *Metallurgical Trans.*, Vol. 16A, pp. 953-969
- [14] Turnbull, A., 1982, "A Theoretical Evaluation of the Influence of Mechanical Variables on the Concentration of Oxygen in a Corrosion Fatigue Crack," *Corrosion Science*, Vol.22, pp. 877-893.
- [15] Darcis, Philippe P., Marines-Garcia, Israel, Hudak, Stephen J. Jr., Armengol, Mariano, and Quintanilla, Hector M., "Sour Environmentally Assisted Fatigue of Welded SCR Materials – Post-Weld Finishing Treatment Evaluation, 29<sup>th</sup> Int'l. Conf. on Offshore Mechanics and Arctic Engineering, OMAE2010-21026, Shanghai.